

# Grounding Current Dispersion of HVDC Grounding System under Dynamic Seasonal Frozen Soil

Lekai Zou<sup>1</sup>, Fan Yang<sup>1, \*</sup>, Bing Gao<sup>1</sup>, Hanwu Luo<sup>2</sup>, Ligang Ye<sup>2</sup>, and Wenzhen Li<sup>2</sup>

**Abstract**—When a high voltage direct current (HVDC) system works at single line operation mode, a big current will flow into the earth through the grounding system directly. Then the large current can cause damage to surrounding equipment and the environment. Therefore, it is significant to study the current dispersion characteristics of HVDC grounding system. Firstly, a  $\pm 800$  kV HVDC model operated at single line mode is built. The grounding current can be seen as the equivalent current source injecting to the grounding system. Secondly, the current dispersion characteristics of horizontal, cross and ring electrodes are investigated. It proves that the ring grounding electrode shows better current dispersion characteristic. And the double-ring grounding electrode whose ratio of inner and outer rings is controlled at 0.7 to 0.75 can get a better current dispersion characteristic. In addition, a dynamic seasonal frozen soil resistivity changing model is built to study the effects of season on the grounding electrodes. The frozen soil would not only increase the ESP, the resistance to ground, and step voltage, but also reduce the current density and electrical field. When the frozen soil is melting, the current dispersion characteristics are the best. The results provide meaningful reference for the design of the grounding system in extremely cold regions.

## 1. INTRODUCTION

In recent years, HVDC transmission system has developed rapidly, not only in quantity but also in voltage levels [1]. However, at the beginning of the construction of an HVDC system, single line transmission mode is used for a period. Double line operation mode is adopted after the completion of the HVDC system [2]. In the single line transmission mode, the grounding electrode and the earth form a loop for HVDC transmission. Large DC current flows directly into the earth through the grounding electrode, and the grounding electrode operates in an active state for a long time [3, 4]. In this case, preventing the damage caused by the large grounding current to the surrounding equipment and the buried metal pipeline is a serious problem, which is essential to be solved urgently [5–7]. Therefore, it is necessary to calculate and analyze the current dispersion characteristics of the HVDC grounding electrode in order to ensure the safe operation of the grounding electrode and minimize its damage on the surrounding environment [8, 9].

After determining the HVDC line, the current dispersion characteristics of the grounding electrodes are affected by the shape of the electrodes and the soil electrical parameters [10]. There are many shapes of grounding electrode, such as horizontal electrode, cross electrode, and ring electrode [11]. Some works have been done to analyze the characteristic of some kinds of grounding electrode [12–14]. For example, Ref. [12] evaluates the electrical voltage and current density in the immediate vicinity of a toroidal grounding installation of DC substations. Ref. [13] studies the effect of impurities on performance of

---

*Received 19 April 2020, Accepted 18 June 2020, Scheduled 9 July 2020*

\* Corresponding author: Fan Yang (yangfan@cqu.edu.cn).

<sup>1</sup> State Key Laboratory of Power Transmission Equipment & System Security and New Technology, School of Electrical Engineering, Chongqing University, Chongqing 400044, China. <sup>2</sup> State Grid East Inner Mongolia Electric Power Maintenance Company, Tongliao 028000, China.

HVDC cross grounding electrode. Ref. [14] analyzes the performance of the circle high-voltage direct current (HVDC) grounding system buried in the horizontal multilayer soil. However, they only analyze the current dispersion effect of one or two kinds of grounding electrodes. And there is no comparison in different shapes of grounding electrode.

In addition, there are permafrost and seasonal frozen soil in the extremely cold regions. When constructing HVDC grounding systems in these areas, apart from considering the shape and depth of the grounding electrode, the effects of frozen soil must also be considered [15–18]. Ref. [15] analyzes the influences of the frozen soil on the optimal design of grounding systems in homogeneous and double-layer soil models. Ref. [16] studies the conductivity and lightning impulse breakdown characteristics of frozen soil and compares it with conventional soil. In reality, the resistivity of seasonal frozen soil during formation and melting process is complicated. The influence of every state of frozen soil on the grounding electrodes should be analyzed.

In this paper, an equivalent  $\pm 800$  kV HVDC transmission model is established firstly, and the grounding current of the HVDC system in stable operation state is obtained. Then the ESP and current density of horizontal, cross and ring electrodes are studied with multi-layered soil structure. The results indicate that the ring grounding electrode has relatively good current dispersion characteristics, hence, the ring grounding electrodes with different numbers of rings are further analyzed. Finally, a dynamic seasonal frozen soil resistivity changing model including the process of icing soil and melting soil is established, and the influence of soil electrical parameters on the current dispersion characteristics is analyzed. We find that the current dispersion effects of different shapes of grounding electrodes vary greatly, and the effect of double-ring grounding electrodes performs well. Besides, frozen soil will increase the earth surface potential (ESP) and reduces the surface current density. In order to reduce the damage of frozen soil, the buried depth of the grounding electrode can be increased to make it deeper than the maximum depth of frozen soil.

## 2. THE GREEN'S FUNCTION OF MULTI-LEVEL HORIZONTAL SOIL

As shown in Figure 1, the current source is located in the multi-layer horizontal soil using a cylindrical coordinate system to analyze [11, 19, 20]. And the Green's function is used to calculate the potential caused by the point current source [20].

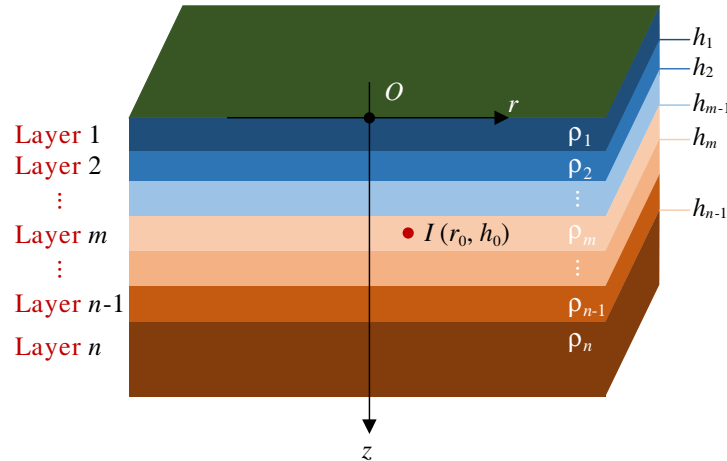


**Figure 1.** Schematic diagram of the Green's function in multi-layer horizontal soil.

We can see in Figure 1 that  $I$  is the current source, and  $(r_0, h_0)$  indicates its location.  $\rho_i$  indicates the resistivity ( $\Omega \cdot m$ ), and  $h_i$  indicates the thickness ( $m$ ) of the  $i$  layer soil.  $(r, z)$  is the observation point.  $m$  ( $1 \leq m \leq n$ ) indicates which layer the current  $I$  is on. The Poisson equation for the space potential is [21]:

$$\frac{\partial^2 \phi}{\partial r^2} + \frac{1}{r} \frac{\partial \phi}{\partial r} + \frac{\partial^2 \phi}{\partial z^2} = -\rho_m \delta \left( \sqrt{|\bar{r} - \bar{r}_0|^2 + (z - h_0)^2} \right) \quad (1)$$

$$\phi_i^m(r, z) = \frac{\rho_i}{4\pi} \int_0^{+\infty} \left( \delta(m-i)e^{-\lambda|z-h_0|} A_i^m(\lambda)e^{-\lambda(z-h_0)} + B_i^m(\lambda)e^{-\lambda(z-h_0)} \cdot J_0(\lambda|\bar{r} - \bar{r}_0|) \right) d\lambda \quad (2)$$

In this formula,  $\delta$  is the Dirac Delta function. Eq. (2) is Hankel transform numerical integration.  $\phi_i^m(r, z)$  indicates the space potential function  $\phi$ .  $J_0$  is the Bessel function of the first kind.  $A_i^m$  and  $B_i^m$  are the function of the integral variable  $\lambda$  [22].

The boundary conditions are known as follows:

$$z = 0, \quad \frac{\partial \phi_1^m}{\partial z} = 0. \quad (3)$$

$$z \rightarrow +\infty; \quad \phi_n^m = 0. \quad (4)$$

$$z = h_i, \quad \phi_i^m = \phi_{i+1}^m, \quad \frac{1}{\rho_i} \frac{\partial \phi_i^m}{\partial z} = \frac{1}{\rho_{i+1}} \frac{\partial \phi_{i+1}^m}{\partial z}, \quad i = 1, \dots, n - 1. \quad (5)$$

We can get  $2n$  equations from these conditions. If it exists  $\lambda_1, \lambda_2, \dots, \lambda_l$ , then solving these equations can get  $A_i^m(\lambda_j)$  and  $B_i^m(\lambda_j)$ , ( $j = 1, 2, \dots, l$ ).

### 3. HVDC TRANSMISSION EQUIVALENT MODEL

As shown in Figure 2, a  $\pm 800$  kV HVDC transmission equivalent model with single line is built in MATLAB. It includes a generator, a transformer, a rectifier, an inverter, AC filters, a DC transmission line, grounding, inverter control and protection, rectifier control and protection, master control, and oscilloscope [11, 23].

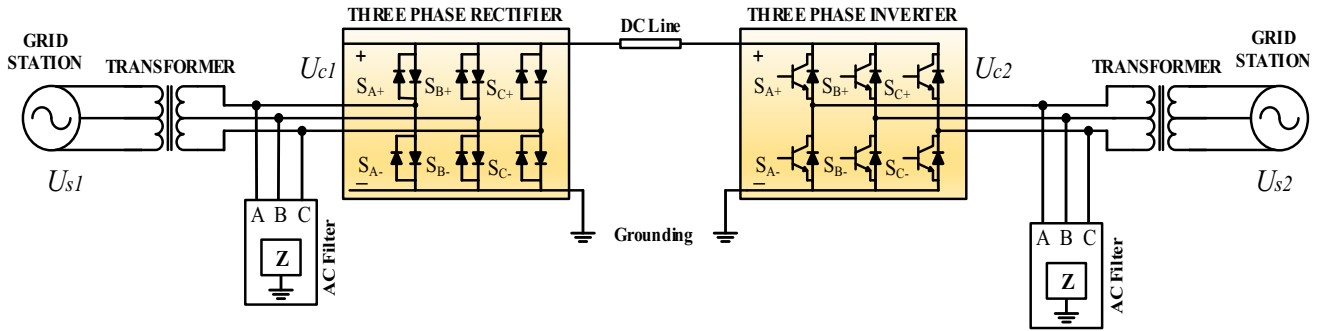
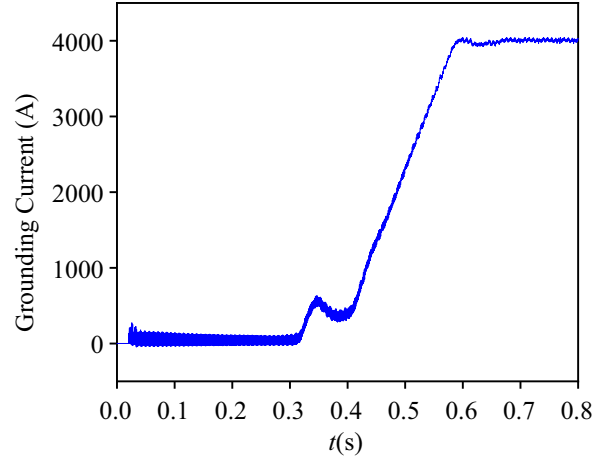


Figure 2. Equivalent circuit model of single line HVDC transmission system.

Figure 3 shows the HVDC grounding current from the operation to the stabilization. After the system is running, the ground current gradually increases and reaches stability at 0.6 s. We focus on the grounding current dispersion characteristic under stable operation (after 0.6 s). So this steady current (4000 A) can be seen as the equivalent current source injected into the grounding system when the system is in normal operation. The current source injected to all grounding electrodes is the same in this paper, and the source impedance has the same effect on all grounding electrodes. Therefore, the influence of the source impedance on the current dispersion characteristic of grounding electrodes is ignored. Ground current is usually divided into multiple currents by many diversion cables. Each electrode of the grounding electrodes is connected by a diversion cable. When the number of diversion cables is sufficient and the current shunt sufficiently uniform, the current dispersion characteristics will be the best, and the influence caused by resistance of the diversion cables on the grounding electrodes will be ignored.



**Figure 3.** Grounding current in single line HVDC system from beginning to 0.8 s.

## 4. CURRENT DISPERSION CHARACTERISTIC OF COMMON GROUNDING ELECTRODES

### 4.1. Three Common Kinds of Grounding Electrodes

There are three common types of grounding electrodes, which are horizontal electrode, cross electrode, and ring electrode [11]. We compare these three types of grounding electrodes and look for the best grounding electrode for the current dispersion. The equivalent current source obtained from Figure 3 is injected to horizontal, cross, and ring grounding electrodes. The depth of burying is 10 m, and all grounding electrodes are calculated under the three-layer vertical layered soil model which is given by State Grid East Inner Mongolia Electric Power Maintenance Company as shown in Table 1. There is air above the first layer of the soil. The resistivity of surface soil is  $354.8528 \Omega \cdot \text{m}$ , and the depth is 1.802306 m. The resistivity of the second layer of soil is  $63.16796 \Omega \cdot \text{m}$ , and the depth is 10.04796 m. The resistivity of the bottom soil is  $65.03293 \Omega \cdot \text{m}$ .

**Table 1.** 3-layer soil model for calculating grounding electrodes current dispersion characteristic.

Layer Number	Resistivity ( $\Omega \cdot \text{m}$ )	Thickness (m)
1	354.8528	1.802306
2	63.16796	10.04796
3	65.03293	Infinite

CDEGS developed by SES of Canada is a powerful tool for solving engineering problems such as Soil Structure Analysis, grounding, and electromagnetic fields  $e$  [24–26]. Firstly, a 400 m horizontal electrode model is built as shown in Figure 4(a). The buried depth  $h$  is 10 m, and the cross-sectional area of the electrodes is  $60 \text{ mm}^2$ . Then the equivalent current source (4000 A) is injected to the center of the electrode. We can see from Figure 4(a) that the ESP distribution of horizontal electrode is symmetrical. The ESP above the grounding electrode is the highest, and the maximum value of ESP is 751.2 V. The ESP decreases rapidly between 200 m and 400 m near the electrode. But after 400 m, the trend of the ESP reduction is slowing down. The value of ESP is 42.2 V in 1000 m.

Then a cross grounding electrode mode is built. It consists of two horizontal electrodes placed vertically, and the length of each electrode is 400 m. The buried depth  $h$  is 10 m, and the cross-sectional area of the electrodes is  $60 \text{ mm}^2$ . The same equivalent current source (4000 A) is injected to the junction. Figure 4(b) shows the ESP distribution of the cross electrode. The maximum ESP is in the earth surface

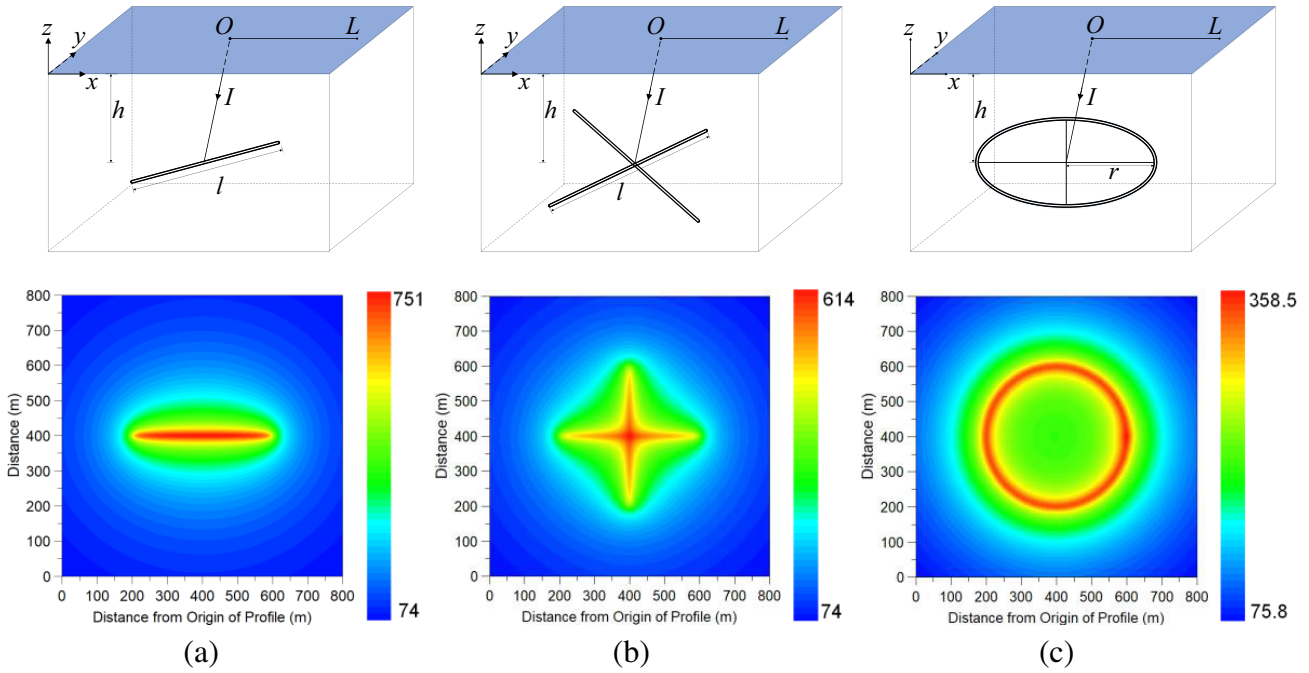


**Figure 4.** The ESP distribution of three common kinds of electrodes. (a) ESP distribution of horizontal electrode; (b) ESP distribution of cross electrode; (c) ESP distribution of ring electrode.

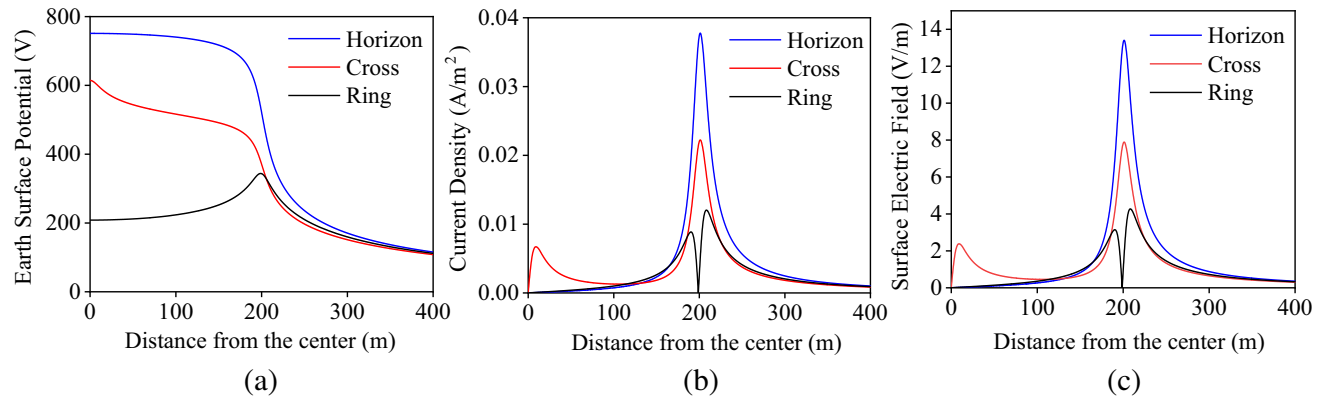


**Figure 5.** Comparison of current dispersion characteristic with horizontal, cross and ring grounding electrodes. (a) ESP distribution of 3 types of electrodes; (b) Surface current density distribution of 3 types of electrodes; (c) Surface electric field of 3 types of electrodes.

above the center of the cross grounding electrode which is 614.4 V. The ESP is reduced rapidly from 371.1 V to 108.0 V from 200 m to 400 m. And in an area far from the electrode, the trend of the ESP reduction is also dropped gently. The value of ESP is 41.8 V in 1000 m.

Figure 4(c) shows a 400 m diameter ring electrode mode and its ESP distribution. The buried depth  $h$  is 10 m, and the cross-sectional area of the electrodes is  $60 \text{ mm}^2$ . The ESP is symmetrically distributed in the surface because of the symmetry of the ring grounding electrode. The maximum ESP is 343.8 V evenly distributed directly above the electrode. From 0 to 200 m, the ESP shows a rapid upward trend. Different from the horizontal and cross electrodes, the ESP in the center is much lower which is 208.2 V because there is no electrode in this area and no current injected to the center. The ESP shows a smooth decline trend after 400 m. The value of ESP is 42.0 V in 1000 m.

Figure 5(a) shows the ESP distribution of horizontal, cross, and ring electrodes from 0 to 400 m

in observation line  $L$  on the earth surface. The ESP of the horizontal electrode is the highest in all positions. And the ESP of the cross electrode is higher than the ring electrode from 0 to 200 m. After a distance of 200 m, the ESP of the cross electrode is less than the ESP of ring electrodes. Although the ESP distribution characteristics and these maximum values are totally different, the ESPs of the three types of ground electrodes are much different in the area far away from center. The ESPs of the three grounded electrodes at the 1000 m are 42.2 V, 41.8 V, and 42.0 V, respectively. When studying the effects of grounding electrodes on the equipment at a great distance, the shape of grounding electrode has little effect on it.

It can be found from Figure 5(b) and Figure 5(c) that the trends of the surface electric field and surface current density are the same. The horizontal electrode has both the highest ESP and the highest current density. The maximum current density of the horizontal and cross electrodes is in 200 m (37.38 mA/m<sup>2</sup> for horizontal electrode and 22.00 mA/m<sup>2</sup> for cross electrode). Then the curves decrease quickly on both sides of 200 m. But the ring grounding electrode shows a completely different current density distribution compared with horizontal electrode and cross electrode. The current density is  $6.13 \times 10^{-7}$  mA/m<sup>2</sup> at 0 m in observation line  $L$  which is the center of the electrode. The reason for the current close to 0 is that the electrodes are centrosymmetric, and the currents flowing through the center of the ring electrode cancel each other out. The horizontal component current is completely cancelled. Only a small vertical component current remains at the ring center. The current density of cross electrode increases suddenly in 9.3 m which is near the junction of electrodes and the injection of grounding current. In the area away from the grounding electrodes, we can see from Table 2 that the values of the current density tend to be similar and gentle as the distance increased. So, the ring electrode has more stable ESP, better current density distribution and resistance-to-ground. It is found that the calculation results in this paper can accurately reflect the current dispersion characteristics of grounding electrodes by comparing with the conclusions in [27, 28].

**Table 2.** 300–1000 m surface current density distribution of horizontal, cross and ring electrode.

Electrode Type	Resistance-to-ground ( $\Omega$ )	Maximum ESP (V)	Maximum Step Voltage (V)	Surface Current Density (mA/m <sup>2</sup> )			
				400 m	600 m	800 m	1000 m
Horizon	0.27635	751.2	10.83	1.00	0.370	0.197	0.122
Cross	0.17680	614.4	6.34	0.837	0.340	0.187	0.119
Single Ring	0.11487	343.8	3.46	0.910	0.356	0.192	0.121

## 4.2. Ring Grounding System

From the above research, we can see that the ring grounding electrode has good current dispersion performance relatively. In this section, the dispersion characteristics of ring grounding electrodes are further analyzed, and the computation and comparison of ring grounding electrode with different numbers of rings are conducted.

Then the equivalent current source obtained from Figure 2 is injected to three common types of ring grounding electrodes as shown in Figure 6 [9]. The ring grounding electrodes are buried in the same three-layer soil model which can be seen in Table 1. The burying depth  $h$  is 10 m, and the cross-sectional area of the electrodes is 60 mm<sup>2</sup>.

First, a single-ring electrode model with 200 m radius is built, and the equivalent current source (4000 A) is injected to the electrode. The resistance-to-ground of single-ring electrode is 0.11487  $\Omega$ . Figure 6(a) shows its ESP distribution, and the maximum ESP is 343.6 V equably distributed over the ring. As mentioned in previous section, the ESP in the center is much lower which is 207.7 V. The ESP has a gentle upward trend from 0 to 200 m. After 200 m, the trend of ESP also drops flattened. The ESP is 42.0 V in 1000 m.

Then we build a double-ring electrode mode shown in Figure 6(b). It includes an inner ring and an outer ring. The radius of the inner ring is  $r_1$ , and the radius of the inner ring is  $r_2$ . The radius of the outer ring ( $r_2$ ) is fixed to 200 m, and the radius of the inner ring ( $r_1$ ) varies from 50 m to 180 m.

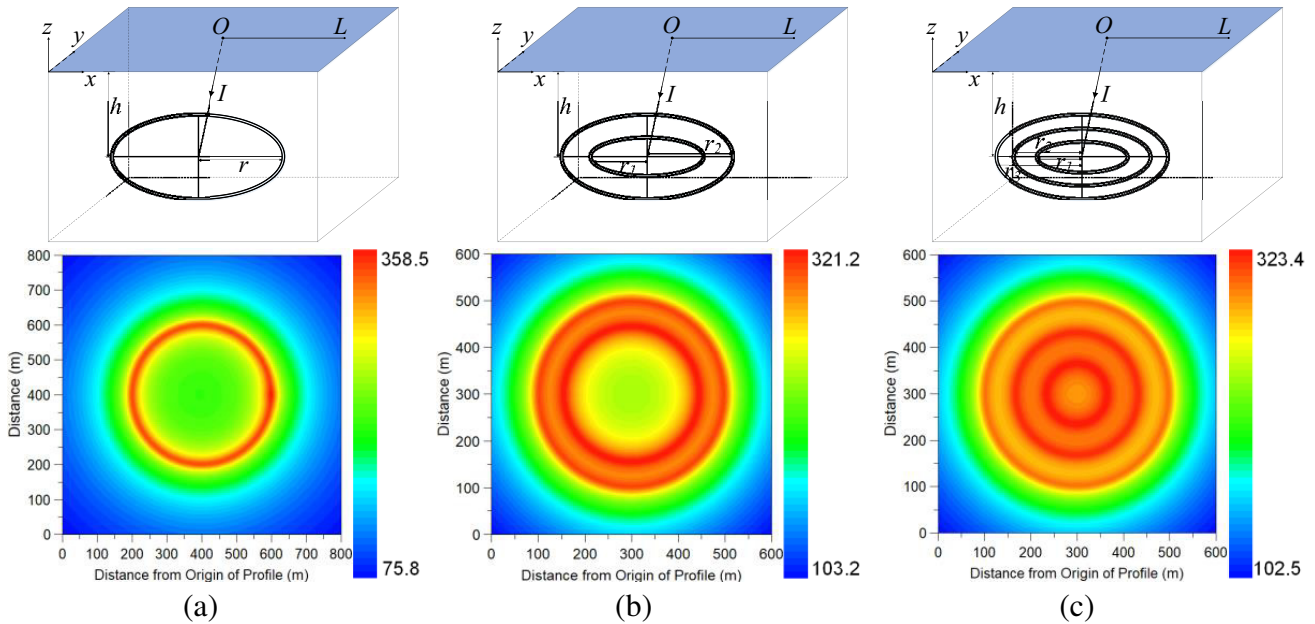


**Figure 6.** Structures and ESP distribution of ring electrode. (a) A 200 m radius single-ring grounding electrode; (b) Double-ring grounding electrode with 145 m radius of inner ring and 200 m radius of outer ring; (c) Triple-ring grounding electrode with 66.67 m radius of inner ring, 133.33 m radius of middle ring and 200 m radius of outer ring.

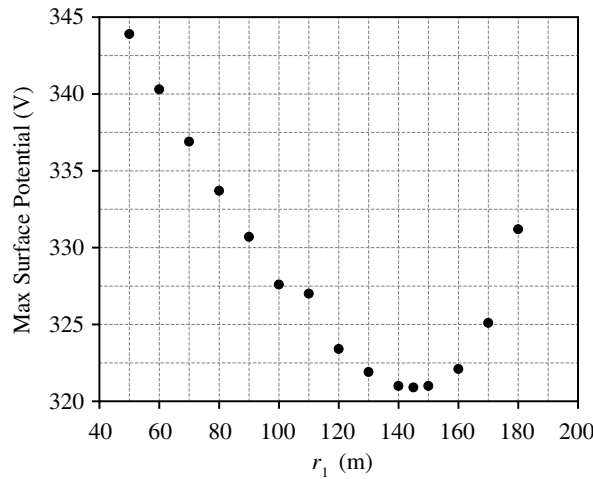


**Figure 7.** Maximum ESP with  $r_1$  changing from 50 m to 180 m and  $r_2$  is fixed to 200 m.

Figure 7 shows the maximum ESP with changing  $r_1$ . When  $r_2$  is 140 m and 150 m, the ESP is the smallest, about 325.5 to 323.8 V. It means that the ESP distribution is the best when the ratio of inner and outer ring radii is 0.70 to 0.75. So, the best radius of inner ring is 145 m, and the ESP distribution is shown in Figure 6(b). The resistance-to-ground of double-ring electrode is  $0.095862 \Omega$ . The maximum ESP above the inner ring is 320.9 V, and the ESP above the outer ring is 307.2 V which is much lower than the maximum value in single-ring electrode. Besides, the ESP above the outer ring is smaller than that when using a single-ring. The ESP distribution is smoother inside the grounding electrode, and the value is smaller after 200 m.

A triple ring grounding electrode model is also built, and the structure is shown in Figure 6(c). The resistance-to-ground of triple-ring electrode is  $0.092513 \Omega$ . The ESP above the electrode is higher

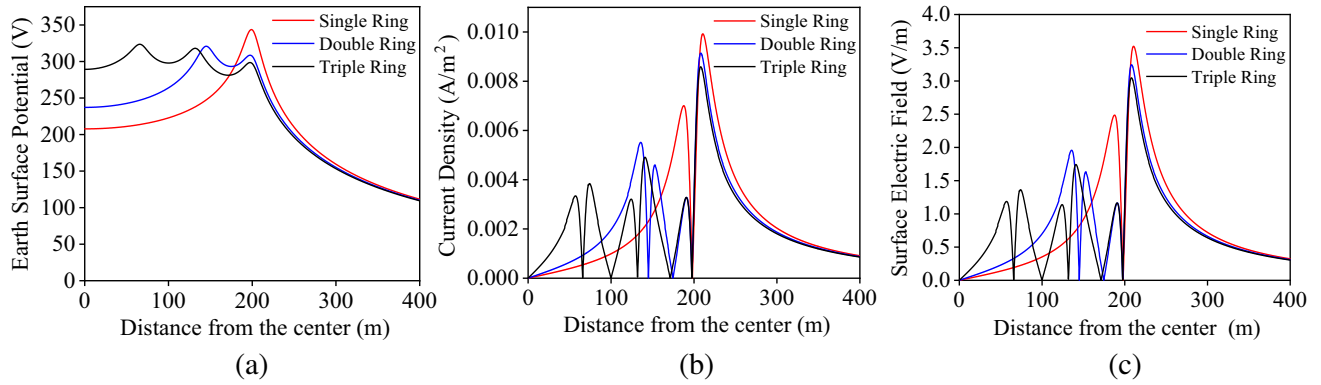


**Figure 8.** Comparison of current dispersion characteristic with three kinds of ring grounding electrodes. (a) ESP distribution of three kinds of ring electrodes; (b) Surface current density distribution of three kinds of ring grounding electrodes; (c) Surface electric field of three kinds of ring electrodes.

than that in other places. The maximum value is above the inner ring which is 323.5 V. The ESP above the middle ring electrode is 318.0, and that above the outer ring is 298.4 in 200 m. Compared with single-ring and double-ring electrodes, although the ESP is smaller for outside the outer ring case, the ESP is much higher within the range of the grounding electrode.

The ESP distribution and current density distribution from the center to 400 m on the earth surface are drawn in Figure 8. Although single-ring electrode has a low ESP in the central region, the ESP is higher than the other 2 types of electrodes in the outside of the electrode area. In addition, the maximum ESP in double-ring electrode is smaller than other two types of electrodes, but double-ring electrode has higher ESP distribution after 138.4 m. Triple ring electrode has the highest ESP distribution near the center because the inner ring is close to the center.

We can see from Figure 8(b) that the value of current density above the electrode is the smallest, but the value on either side of the electrode is much higher. With the increase of the number of electrode rings, the distribution of surface current density inside the electrode is more complex, and the current density outside the electrode is lower. The surface current density distribution has a trough at 200 m ( $2.02 \text{ mA/m}^2$ ) which is above the ring electrode, and there are two peaks on each side of 200 m. Then we plot the surface current density in the three directions of  $x, y, z$  on the observation line  $L$  at the same position in Figure 9 to figure out why there is a trough and two peaks near 200 m. The surface current density in the  $y$  and  $z$  directions is small. The surface current density in the  $x$  direction is much greater than the surface current density in other two directions and plays a dominant role on the surface. Figure 9(a) shows that the direction of surface current density is toward the center of the ring electrode from 0 to 200 m in  $x$  direction, and the value of surface current density is 0 at 200 m. The direction of the surface current density in  $x$  direction changes at 200 m. Then the direction of surface current density is toward the outside of the ring electrode after 200 m in  $x$  direction. So, there are a trough at 200 m and two peaks near 200 m in ring grounding. The direction of the surface current density of double-ring grounding electrode in  $x$  direction changes 2 times. There are 2 troughs above each ring and 4 peaks for double-ring grounding electrode. The direction of the surface current density of triple-ring grounding electrode in  $x$  direction changes 3 times. There are 3 troughs above each ring and 6 peaks for triple-ring grounding electrode. The trends of the surface electric field and surface current density are the same.

In general, the triple ring grounding electrode has the best dispersion effect, and the single-ring grounding electrode has the least dispersion effect. However, the triple ring grounding electrode requires more materials and higher cost. It is recommended that the double-ring ground electrode is considered first to ensure better dispersion effect and save costs.

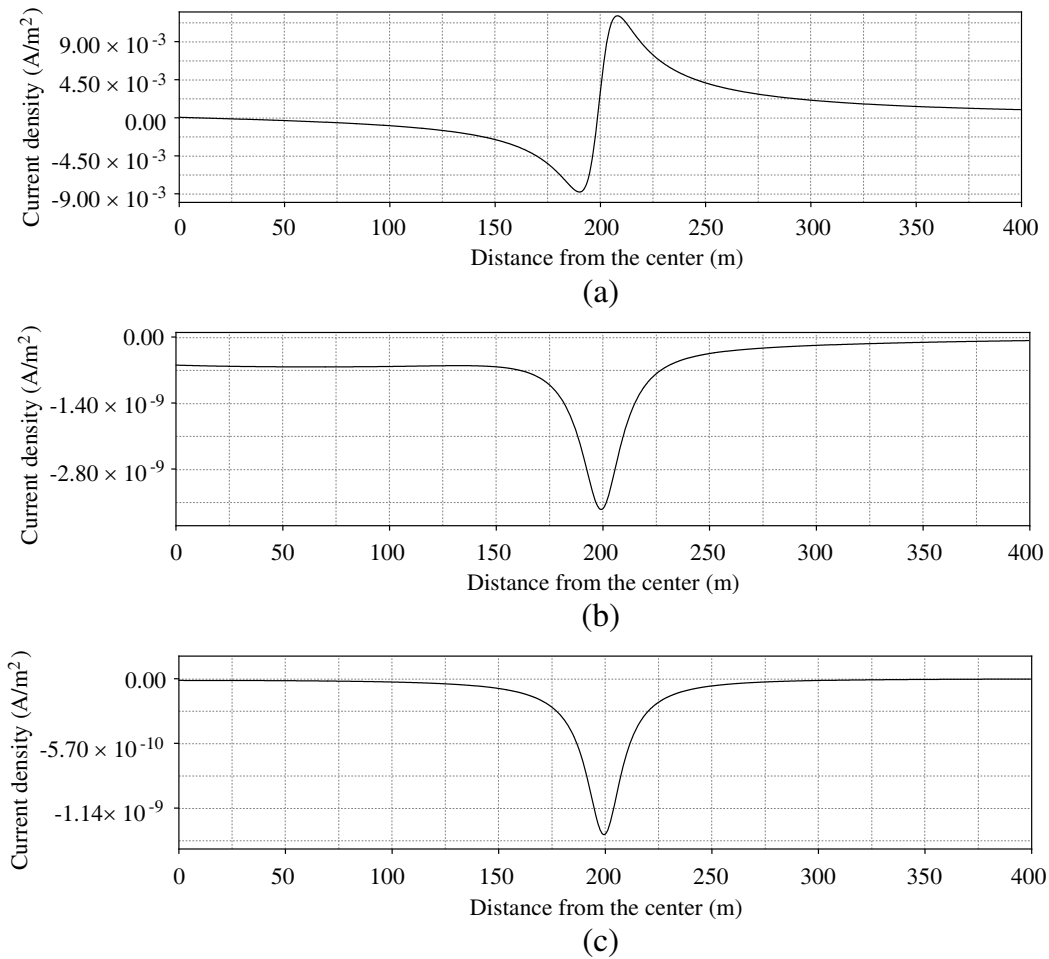


**Figure 9.** Surface current density distribution of ring grounding electrode in 3 three directions. (a) Surface current density distribution of ring grounding electrode in  $x$  direction; (b) Surface current density distribution of ring grounding electrode in  $y$  direction; (c) Surface current density distribution of ring grounding electrode in  $z$  direction.

### 5. CURRENT DISPERSION CHARACTERISTIC OF GROUNDING ELECTRODE UNDER DYNAMIC SEASONAL FROZEN SOIL

When the frozen soil is forming, the resistivity of surface soil will increase significantly, which will greatly affect the grounding current dispersion characteristics [26]. In this section, a dynamic seasonal frozen soil model is modeled to analyze the influence of soil. Figure 10 shows the transformation of dynamic seasonal frozen soil in different periods. In extremely cold regions, the normal soil mode is usually between July and August every year. The frozen soil mode is between September and November. The frozen soil pattern is between December and April of the following year. The melting soil mode is between May and June. A thin layer of frozen soil is expected in the surface of the soil for frozen condition, and the maximum freezing depth would keep stable after a period of time [29]. With the atmospheric temperature rising, the frozen soil melts, and the surface frozen soil melts first. At this time, the surface layer and deep layer are non-frozen soil, but the middle layer is still frozen soil. After a period of time, the frozen soil is completely melted to the normal soil mode [30]. Consequently, the dynamic grounding current dispersion characteristics under the above cases are investigated.

Table 3 shows the resistivity stratification data of the dynamic seasonal frozen soil model at each stage. The maximum depth of frozen soil is 1.6 m. We set the resistivity of permafrost to  $5000 \Omega \cdot m$

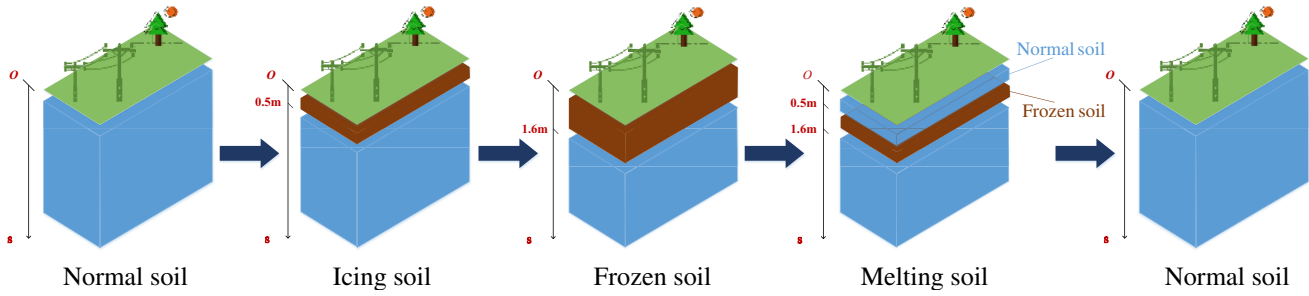


**Figure 10.** Schematic diagram of dynamic seasonal frozen soil change process.

and the resistivity of non-frozen soil to  $160 \Omega \cdot m$  [15]. The icing soil mode is the period when the soil is forming permafrost, and the frozen soil mode is the period when the soil has formed permafrost. Table 3 shows that the frozen and icing soils have the same resistivity values ( $5000 \Omega \cdot m$ ) in the first layer. But the thickness of the first layer is different. The thickness of the first layer in icing soil mode is 0.5 m, and the thickness of first layer in frozen soil mode is 1.6 m. Then the effect on the dynamic seasonal frozen soil model on the current dispersion characteristics of the grounding electrode is studied.

**Table 3.** Resistivity stratification of dynamic seasonal frozen soil model under different modes.

Mode	Normal soil mode		Icing soil mode		Frozen soil mode		Melting soil mode	
	Resistivity ( $\Omega \cdot m$ )	Thickness (m)	Resistivity ( $\Omega \cdot m$ )	Thickness (m)	Resistivity ( $\Omega \cdot m$ )	Thickness (m)	Resistivity ( $\Omega \cdot m$ )	Thickness (m)
1			5000	0.5	5000	1.6	160	0.5
2	160	$\infty$					5000	1.1
3			160	$\infty$	160	$\infty$	160	$\infty$

**5.1. Buried in the Frozen Soil Layer**

First, a single-ring grounding electrode with a radius of 200 m is buried at a depth of 1 m [31]. We can see that the grounding electrode is buried shallower than the maximum frozen soil depth from Table 3. And the grounding electrode is buried inside the frozen soil after the formation of frozen soil. In this case, the current dispersion characteristics of the grounding electrode in four soil modes are calculated, and Figure 11 shows the ESP and current density.

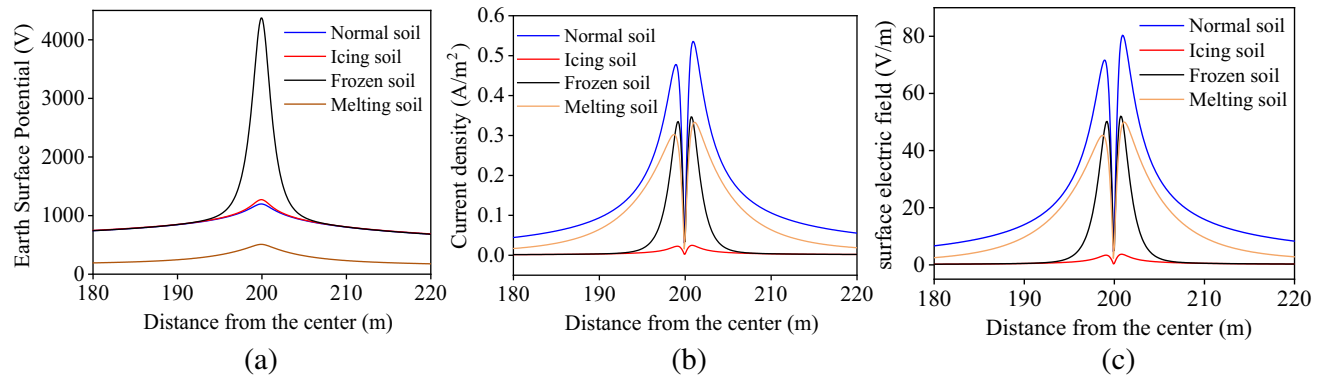


**Figure 11.** Comparison of current dispersion characteristic in four soli mode with grounding electrode buried in 1 m. (a) ESP distribution; (b) Surface current density distribution; (c) Surface electric field.

It can be seen from Figure 11 that the maximum ESP in the frozen soil mode is the largest, which is 3.65 times higher than the ESP in non-frozen soil. And the ESP of the icing soil mode is slightly higher than the ESP of the normal soil mode, because there is a thin layer frozen soil in the earth surface in icing mode. The value has little difference at the center of the grounding electrode and the area far from the grounding electrode. The ESP of the melting soil mode is much smaller than that of the other three modes, mainly because the frozen soil in melting soil mode is in the middle layer, and the grounding electrode is buried in this layer.

The ground electrode has the highest ESP in normal soil mode because there is no frozen layer to prevent current flow. And the icing soil has the lowest ground current density. The current densities of the frozen soil and melting soil modes are not much different but are both higher than that of the icing soil mode.

### 5.2. Buried under the Frozen Soil

Then the ring grounding electrode with a radius of 200 m is buried at a depth of 2 m which is under the frozen soil layer. Figure 12 shows the current dispersion characteristics of the four soli modes.

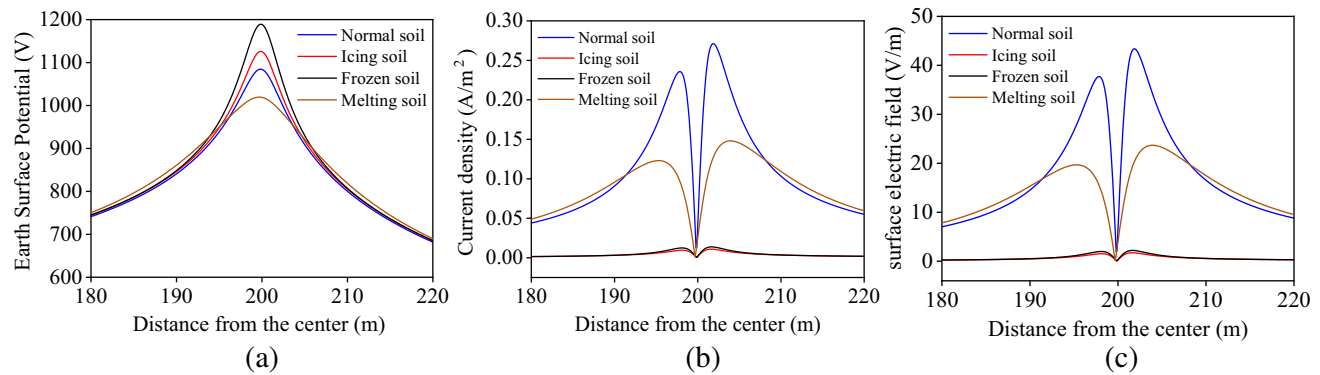


**Figure 12.** Comparison of current dispersion characteristic in four soli mode with grounding electrode buried in 2 m. (a) ESP distribution; (b) Surface current density distribution; (c) Surface electric field.

Compared with the grounding electrode buried with the depth of 1 m, the ESP of the frozen soil mode increases slightly in this case which is only 104.6 V larger than the normal soil mode. And the maximum ESP in the melting soil mode is smaller than the other three modes, but it is higher than the other three modes in the area away from the grounding electrode. It means that the ESP distribution in the melting mode is gentler, and the step voltage is also minimized.

Figure 12(b) shows the current density distribution under four modes. We can see that the distribution of current density with grounding electrode buried in 2 m is totally different from that buried in 1 m. The maximum current density of normal soil is the highest. And the surface current density values of frozen soil and icing soil modes are almost the same because there is frozen soil in the surface of these two modes.

From Figure 11, Figure 12, and Table 4, we can find that the buried depth has a serious effect on current dispersion characteristic of the grounding electrode. Increasing the burial depth will reduce the ESP and resistance-to-ground of the grounding electrodes significantly.

**Table 4.** The resistance-to-ground of the grounding system in 4 modes.

Depth	Normal soil mode	Icing soil mode	Frozen soil mode	Melting soil mode
1 m	0.33096 Ω	0.34684 Ω	1.96380 Ω	0.33588 Ω
2 m	0.31739 Ω	0.32488 Ω	0.35012 Ω	0.34507 Ω

## 6. CONCLUSION

In this paper, a  $\pm 800$  kV HVDC transmission model operated in single line mode is established to calculate the grounding current. This current is used as the equivalent current source to analyze the current dispersion characteristic of some common types of grounding electrodes. A dynamic seasonal frozen soil model is built to study the current dispersion characteristics in different states of frozen soil. The following conclusions are made.

Horizontal grounding electrode has the worst current dispersion effect but the lowest cost. It can be used in the case that the design requirement is not strict. The ring electrodes have more stable ESP and current density distribution. The double-ring grounding electrode has better current dispersion characteristics when the ratio of inner and outer ring radii is 0.70 to 0.75.

The frozen soil would not only increase the ESP, grounding resistance, step voltage, and resistance-to-ground, but also reduce the current density. During the different periods of frozen soil, the current dispersion characteristics in the melting soil mode are the best. We can choose to repair or maintain the grounding electrode during the melting soil season. Increasing the depth of the grounding electrode to make it deeper than the depth of maximum frozen soil can reduce the impact of frozen soil on the grounding electrode.

## ACKNOWLEDGMENT

This research was supported by the science project of state grid (No. SGTYHT/17-JS-199).

## REFERENCES

1. Jian, T., et al., "Analysis of electromagnetic interference on DC line from parallel AC line in close proximity," *IEEE Transactions on Power Delivery*, Vol. 22, No. 4, 2401–2408, 2007.
2. Xiong, R., B. Chen, C. Gao, Y.-X. Li, and W. Yang, "Optimal programs to reduce the resistance of grounding systems," *Progress In Electromagnetics Research*, Vol. 139, 211–227, 2013.
3. Frank, J., "IEEE standard dictionary of electrical and electronics terms," Institute of Electrical and Electronics Engineers, New York, 1988.
4. Ma, J., F. P. Dawalibi, and W. Ruan, "Design considerations of HVDC grounding electrodes," *2005 IEEE/PES Transmission & Distribution Conference & Exposition: Asia and Pacific*, IEEE, 2005.
5. Xiong, R., B. Chen, L.-H. Shi, Y.-T. Duan, and G. Zhang, "An efficient method to reduce the peak transient grounding resistance value of a grounding system," *Progress In Electromagnetics Research*, Vol. 138, 255–267, 2013.
6. Zhang, B., et al., "DC current distribution in both AC power grids and pipelines near HVDC grounding electrode considering their interaction," *IEEE Transactions on Power Delivery*, Vol. 34, No. 6, 2240–2247, 2019.
7. Xiong, R., B. Chen, J.-J. Han, Y.-Y. Qiu, W. Yang, and Q. Ning, "Transient resistance analysis of large grounding systems using the FDTD method," *Progress In Electromagnetics Research*, Vol. 132, 159–175, 2012.
8. Su, L., et al., "The influence of coke aging on electrical performance of double-rings DC grounding electrode," *IOP Conference Series Materials Science and Engineering*, Vol. 452, No. 3, 032072, 2018.
9. Zhang, B., J. He, and R. Zeng, "State of art and prospect of grounding technology in power system," *High Voltage Engineering*, Vol. 41, No. 8, 2569–2582, 2015.
10. Ma, J., F. P. Dawalibi, and W. Ruan, "Design considerations of HVDC grounding electrodes," *2005 IEEE/PES Transmission & Distribution Conference & Exposition: Asia and Pacific*, IEEE, 2005.
11. Luo, H., et al., "Regularity of current dispersal in different kinds of grounding electrode," *2018 IEEE International Conference on High Voltage Engineering and Application (ICHVE)*, IEEE, 2018.

12. Lagace, P. J., et al., "Evaluation of the voltage distribution around toroidal HVDC ground electrodes in N-layer soils," *IEEE Transactions on Power Delivery*, Vol. 3, No. 4, 1573–1579, 1988.
13. Zhang, T., et al., "Effect of backfill soil impurity on electric field characteristics of HVDC grounding-electrode," *2015 IEEE International Conference on Applied Superconductivity and Electromagnetic Devices (ASEMD)*, IEEE, 2015.
14. Zou, J., et al., "Analysis of the toroidal HVDC grounding systems in horizontal multilayer soils," *IEEE Transactions on Magnetics*, Vol. 42, No. 4, 1435–1438, 2006.
15. He, J., et al., "Optimal design of grounding system considering the influence of seasonal frozen soil layer," *IEEE Transactions on Power Delivery*, Vol. 20, No. 1, 107–115, 2005.
16. He, J., et al., "Lightning impulse breakdown characteristics of frozen soil," *IEEE Transactions on Power Delivery*, Vol. 23, No. 4, 2216–2223, 2008.
17. Li, W., et al., "Influence of deep earth resistivity on HVDC ground-return currents distribution," *IEEE Transactions on Power Delivery*, Vol. 32, No. 4, 1844–1851, 2016.
18. Ma, C., et al., "The study on the polar potential distribution of DC grounding in earth structures," *Journal of Physics: Conference Series*, Vol. 1072, No. 1, IOP Publishing, 2018.
19. Pan, Z. H., et al., "Simulation and analysis of earth surface potential distribution in horizontal multi-layer soil," *Gaodiyanya Jishu/High Voltage Engineering*, Vol. 38, No. 1, 116–123, 2012.
20. He, J., R. Zeng, and B. Zhang, "Current field in the earth," *Methodology and Technology for Power System Grounding*, John Wiley & Sons Singapore Pte. Ltd., 2012.
21. Zhang, T., et al., "Effect of backfill soil impurity on electric field characteristics of HVDC grounding-electrode," *2015 IEEE International Conference on Applied Superconductivity and Electromagnetic Devices (ASEMD)*, IEEE, 2015.
22. Zhu, M. and G. Li, "Design principle of flexible protected controller for modular multilevel converter under unbalanced grid conditions," *IEEE Transactions on Electrical and Electronic Engineering*, Vol. 13, No. 4, 570–579, 2018.
23. Chiheb, S., et al., "Transient behavior of vertical grounding electrode under impulse current," *2017 5th International Conference on Electrical Engineering-Boumerdes (ICEE-B)*, IEEE, 2017.
24. Phayomhom, A. and S. Sirisumrannukul, "Safety analysis for grounding system of two neighbouring substations in MEA's power distribution system," *Electrical Engineering Congress*, IEEE, 2014.
25. He, J., R. Zeng, and B. Zhang, "Impulse characteristics of grounding devices," *Methodology and Technology for Power System Grounding*, 1st Edition, 303–390, Wiley-IEEE Press, 2012.
26. He, J., et al., "Fault current-division factor of substation grounding grid in seasonal frozen soil," *IEEE Transactions on Power Delivery*, Vol. 28, No. 2, 855–865, 2013.
27. Ma, J., L. Liu, and S. Sun, "Calculation of earth surface potential distribution of HVDC due to finite element and multi-layer soil," *2011 International Conference on Electrical and Control Engineering*, IEEE, 2011.
28. Prasad, D. and H. C. Sharma, "Soil resistivity and earthing system," *IJMIE*, Vol. 2, No. 9, 369–380, 2012.
29. Si, Y., et al., "DC grounding electrode potential based on a kriging geoelectric structure model," *IEEE Access*, Vol. 7, 166337–166352, 2019.
30. Mondal, M., et al., "Design and analysis of substation grounding grid with and without considering seasonal factors using EDSA software," *International Journal of Innovations in Engineering and Technology*, 64–77, 2012.
31. He, J., R. Zeng, and B. Zhang, "DC ground electrode," *Methodology and Technology for Power System Grounding*, 2012.